Eur. Phys. J. B **32**, 203–214 (2003)
DOI: 10.1140/epjb/e2003-00090-x

THE EUROPEAN PHYSICAL JOURNAL B

Two-dimensional t-J model at moderate doping

A. Sherman[1,a] and M. Schreiber[2]

[1] Institute of Physics, University of Tartu, Riia 142, 51014 Tartu, Estonia
[2] Institut für Physik, Technische Universität, 09107 Chemnitz, Federal Republic of Germany and School of Engineering and Science, International University Bremen, Campus Ring 1, 28759 Bremen, Federal Republic of Germany

Received 14 November 2002
Published online 1st April 2003 –

Abstract. Using the method which retains the rotation symmetry of spin components in the paramagnetic state and has no preset magnetic ordering, spectral and magnetic properties of the two-dimensional t-J model in the normal state are investigated for the ranges of hole concentrations $0 \leq x \leq 0.16$ and temperatures $0.01t \leq T \leq 0.2t$. The used hopping t and exchange J parameters of the model correspond to hole-doped cuprates. The obtained solutions are homogeneous which indicates that stripes and other types of phase separation are not connected with the strong electron correlations described by the model. A series of nearly equidistant maxima in the hole spectral function calculated for low T and x is connected with hole vibrations in the region of the perturbed short-range antiferromagnetic order. The hole spectrum has a pseudogap in the vicinity of $(0, \pi)$ and $(\pi, 0)$. For $x \approx 0.05$ the shape of the hole Fermi surface is transformed from four small ellipses around $(\pm\pi/2, \pm\pi/2)$ to two large rhombuses centered at $(0, 0)$ and (π, π). The calculated temperature and concentration dependencies of the spin correlation length and the magnetic susceptibility are close to those observed in cuprate perovskites. These results offer explanations for the observed scaling of the static uniform susceptibility and for the changes in the spin-lattice relaxation and spin-echo decay rates in terms of the temperature and doping variations in the spin excitation spectrum of the model.

PACS. 71.10.Fd Lattice fermion models – 74.25.Ha Magnetic properties – 74.25.Jb Electronic structure

1 Introduction

The two-dimensional t-J model was proposed by Anderson [1] for the description of strong electron correlations in CuO_2 planes of perovskite high-T_c superconductors. In reference [2] the similarity of the low-energy part of its spectrum with the spectrum of the realistic three-band Hubbard model was demonstrated. Nowadays the t-J model is one of the most frequently used models for the interpretation of experimental results in cuprates (for a review, see Ref. [3]). Different numerical and analytical methods were used for the investigation of the model. Among these methods are the exact diagonalization of small clusters [4,5], Monte Carlo simulations [6], density matrix renormalization group calculations [7], spin-wave [8,9] and mean-field slave-boson approximations [10]. In spite of the considerable progress made towards the understanding of the properties of the model, the basic issues of its behavior at moderate doping have not yet been completely resolved.

Aiming at a description for this range of concentration in reference [11] a new analytical method was developed which has merits of retaining the rotation symmetry of spin components in the paramagnetic state and of the absence of any preset magnetic ordering. Since the description is carried out in terms of the Hubbard operators, the method takes proper account of the kinematic interaction. The method is based on Mori's projection operator technique [12] which allows one to represent Green's functions in the form of continued fractions and gives a way for calculating their elements. The residual term of the fraction is approximated by the decoupling which reduces this many-particle Green's function to a product of the sought-for functions. Using the idea of reference [13] the decoupling is corrected by introducing a vertex correction, a multiplier which is determined from the sum rule of the considered problem, the constraint of zero site magnetization in the paramagnetic state. Test calculations with this method for small clusters and high temperatures demonstrated good agreement of the obtained results with the exact diagonalization and Monte Carlo data. Notice that close approaches which use equations of motion and Tserkovnikov's formalism were developed in reference [14]

[a] e-mail: alexei@fi.tartu.ee

to consider magnetic properties of the 2D t-J model.

This article contains results of calculations carried out with the method of reference [11] for a 20×20 lattice and parameters $J = 0.1$ eV, $t = 0.5$ eV where J and t are the exchange and hopping constants of the t-J model. Test calculations with lattices of other sizes showed that the considered lattice is large enough to avoid finite-size effects in spectral functions. The parameters chosen correspond to hole-doped cuprate perovskites [15]. The considered range of hole concentrations $0 \leq x \leq 0.16$ spans the cases from light to moderate doping. The temperature range of the calculations $0.01t \approx 58\,\mathrm{K} \leq T \leq 0.2t \approx 1200\,\mathrm{K}$ embraces the range of temperatures used in experiment.

The calculated Green's functions reveal a number of peculiarities in the hole and spin excitation spectrum. For low x and T, besides the spin-polaron peak [3], a series of less intensive and broader maxima is observed at higher frequencies in the hole spectral function. These maxima are nearly equidistant which allows us to connect them with vibrations of a hole in a region of the perturbed short-range antiferromagnetic order. This region arises due to the hole movement. The lowest of these maxima with a dispersion which mimics the dispersion of the spin-polaron peak is apparently observed in lightly doped $Ca_2CuO_2Cl_2$. For low hole concentrations only the spin-polaron band crosses the Fermi level which leads to the Fermi surface consisting of four ellipses around $(\pm\pi/2, \pm\pi/2)$. For $x \approx 0.05$ the second band, which arises below the Fermi level in the used hole picture, crosses the Fermi level and the Fermi surface acquires new elements – large rhombuses around $(0,0)$ and (π,π). However, due to the peculiar dispersion of the spin-polaron band and its larger spectral intensity parts of this large Fermi surface near $(0,\pi)$ and $(\pi,0)$ are hidden which looks like a pseudogap, a decrease of the low-frequency spectral intensity in these regions of the Brillouin zone. The magnitude of the pseudogap – the energy distance between the spin-polaron peak and the Fermi level – decreases with x and at $x \approx 0.12$ the pseudogap disappears. The symmetry, magnitude and concentration dependence of the calculated pseudogap are similar to those observed in Bi-based cuprates.

As mentioned, the method used has no preset magnetic ordering which opens the way to investigate whether the strong electron correlations described by the t-J model are responsible for the charge and magnetic inhomogeneities observed in some cuprates [16]. In the considered ranges of hole concentrations and temperatures only the homogeneous solutions were found which indicates that other interactions have to be invoked to explain these inhomogeneities.

The calculated spectrum of spin excitations contains a gap near (π,π) which is directly connected with the correlation length of the short-range antiferromagnetic order. The dependence of the correlation length on x reproduces the relation observed experimentally in $La_{2-x}Sr_xCuO_4$ [17]. With increasing x the branch of spin excitations is destroyed near $(0,0)$, whereas at the periphery of the Brillouin zone the excitations remain well defined. The calculated magnetic susceptibility and its dependencies on x and T are similar to those observed in neutron scattering and NMR experiments. This similarity allows us to offer explanations for the observed scaling of the static uniform susceptibility and for the changes in the spin-lattice relaxation and spin-echo decay rates in terms of the temperature and doping variations in the spin excitation spectrum of the t-J model.

For convenience main formulas of reference [11], which were used in the calculations, are reproduced in Section 2. In Sections 3 and 4 peculiarities of the hole and spin excitation spectra are discussed. The spin susceptibility, spin correlations, spin-lattice relaxation and spin-echo decay rates are considered in Section 5. Our conclusions are given in Section 6.

2 Main formulas

The Hamiltonian of the 2D t-J model reads [3]

$$H = \sum_{\mathbf{nm}\sigma} t_{\mathbf{nm}} a^{\dagger}_{\mathbf{n}\sigma} a_{\mathbf{m}\sigma} + \frac{1}{2}\sum_{\mathbf{nm}} J_{\mathbf{nm}} \left(s^z_{\mathbf{n}} s^z_{\mathbf{m}} + s^{+1}_{\mathbf{n}} s^{-1}_{\mathbf{m}} \right), \quad (1)$$

where $a_{\mathbf{n}\sigma} = |\mathbf{n}\sigma\rangle\langle\mathbf{n}0|$ is the hole annihilation operator, $\mathbf{n}$ and $\mathbf{m}$ label sites of the square lattice, $\sigma = \pm 1$ is the spin projection, $|\mathbf{n}\sigma\rangle$ and $|\mathbf{n}0\rangle$ are site states corresponding to the absence and presence of a hole on the site. These states may be considered as linear combinations of the products of the $3d_{x^2-y^2}$ copper and $2p_\sigma$ oxygen orbitals of the extended Hubbard model [8,18]. In this work we take into account nearest neighbor interactions only, $t_{\mathbf{nm}} = -t\sum_{\mathbf{a}} \delta_{\mathbf{n},\mathbf{m}+\mathbf{a}}$ and $J_{\mathbf{nm}} = J\sum_{\mathbf{a}} \delta_{\mathbf{n},\mathbf{m}+\mathbf{a}}$ where the four vectors $\mathbf{a}$ connect nearest neighbor sites. The spin-$\frac{1}{2}$ operators can be written as $s^z_{\mathbf{n}} = \frac{1}{2}\sum_\sigma \sigma |\mathbf{n}\sigma\rangle\langle\mathbf{n}\sigma|$ and $s^\sigma_{\mathbf{n}} = |\mathbf{n}\sigma\rangle\langle\mathbf{n},-\sigma|$.

Due to the complicated commutation relations the diagram technique for the operators $a_{\mathbf{n}\sigma}$, $s^z_{\mathbf{n}}$, and $s^\sigma_{\mathbf{n}}$ is very intricate [19]. In this case the use of Mori's projection operator technique [12] for the derivation of self-energy equations for Green's functions constructed from such operators is especially fruitful. In this way the following equations were found for the hole $G(\mathbf{k}t) = \langle\langle a_{\mathbf{k}\sigma} | a^{\dagger}_{\mathbf{k}\sigma}\rangle\rangle = -\mathrm{i}\theta(t)\langle\{a_{\mathbf{k}\sigma}(t), a^{\dagger}_{\mathbf{k}\sigma}\}\rangle$ and spin $D(\mathbf{k}t) = -\mathrm{i}\theta(t)\langle[s^z_{\mathbf{k}}(t), s^z_{-\mathbf{k}}]\rangle$ Green's functions [11]:

$$D(\mathbf{k}\omega) = \frac{[4J\alpha(\Delta + 1 + \gamma_{\mathbf{k}})]^{-1} \Pi(\mathbf{k}\omega) + 4JC_1(\gamma_{\mathbf{k}} - 1)}{\omega^2 - \Pi(\mathbf{k}\omega) - \omega^2_{\mathbf{k}}}, \quad (2)$$

$$G(\mathbf{k}\omega) = \phi[\omega - \varepsilon_{\mathbf{k}} + \mu - \Sigma(\mathbf{k}\omega)]^{-1},$$

where $D(\mathbf{k}\omega) = \int_{-\infty}^{\infty} \exp(\mathrm{i}\omega t) D(\mathbf{k}t)\mathrm{d}t$,

$$a_{\mathbf{k}\sigma} = N^{-1/2}\sum_{\mathbf{n}} \exp(-\mathrm{i}\mathbf{kn}) a_{\mathbf{n}\sigma},$$

$$s^z_{\mathbf{k}} = N^{-1/2}\sum_{\mathbf{n}} \exp(-\mathrm{i}\mathbf{kn}) s^z_{\mathbf{n}},$$

$a_{\mathbf{k}\sigma}(t) = \exp(\mathrm{i}\mathcal{H}t) a_{\mathbf{k}\sigma} \exp(-\mathrm{i}\mathcal{H}t)$, N is the number of sites, $\mathcal{H} = H - \mu\sum_{\mathbf{n}} X_{\mathbf{n}}$, μ is the chemical potential,

$X_{\mathbf{n}} = |\mathbf{n}0\rangle\langle\mathbf{n}0|$, the angular brackets denote averaging over the grand canonical ensemble, $\gamma_{\mathbf{k}} = \frac{1}{4}\sum_{\mathbf{a}} \exp(\mathrm{i}\mathbf{k}\mathbf{a})$, $\phi = \frac{1}{2}(1+x)$, and

$$\omega_{\mathbf{k}}^2 = 16J^2\alpha|C_1|(1-\gamma_{\mathbf{k}})(\Delta+1+\gamma_{\mathbf{k}}), \tag{3}$$

$$\varepsilon_{\mathbf{k}} = -(4\phi t + 6C_1\phi^{-1}t + 3F_1\phi^{-1}J)\gamma_{\mathbf{k}}.$$

In the present calculations the parameter of vertex correction α, which improves the decoupling in the residual term, is set equal to its value in the undoped case, $\alpha = 1.802$ (this value differs slightly from that reported in references [11,20] due to an artificial broadening introduced in $D(\mathbf{k}\omega)$, see below). The parameter Δ which describes a gap in the spectrum of spin excitations at (π,π) (see Eq. (3)) is determined by the constraint of zero site magnetization $\langle s_{\mathbf{l}}^z\rangle = 0$ in the paramagnetic state. The constraint can be written in the form

$$\frac{1}{2}(1-x) = \frac{2}{N}\sum_{\mathbf{k}}\int_0^\infty \mathrm{d}\omega \coth\Big(\frac{\omega}{2T}\Big) B(\mathbf{k}\omega), \tag{4}$$

where $B(\mathbf{k}\omega) = -\pi^{-1}\mathrm{Im}\, D(\mathbf{k}\omega)$ is the spin spectral function. Notice that in accord with the Mermin-Wagner theorem [21] in the considered 2D system the long-range antiferromagnetic ordering is destroyed at any nonzero T and, as will be seen below, for $T = 0$ and $x > x_c \approx 0.02$. The value of x and the nearest neighbor correlations $C_1 = \langle s_{\mathbf{l}}^{+1} s_{\mathbf{l}+\mathbf{a}}^{-1}\rangle$ and $F_1 = \langle a_{\mathbf{l}}^\dagger a_{\mathbf{l}+\mathbf{a}}\rangle$ are connected with Green's functions (2) by the following relations:

$$\begin{aligned} x &= \frac{1}{N}\sum_{\mathbf{k}}\int_{-\infty}^\infty \mathrm{d}\omega n_F(\omega) A(\mathbf{k}\omega), \\ F_1 &= \frac{1}{N}\sum_{\mathbf{k}}\gamma_{\mathbf{k}}\int_{-\infty}^\infty \mathrm{d}\omega n_F(\omega) A(\mathbf{k}\omega), \\ C_1 &= \frac{2}{N}\sum_{\mathbf{k}}\gamma_{\mathbf{k}}\int_0^\infty \mathrm{d}\omega \coth\Big(\frac{\omega}{2T}\Big) B(\mathbf{k}\omega), \end{aligned} \tag{5}$$

where $A(\mathbf{k}\omega) = -\pi^{-1}\mathrm{Im}\, G(\mathbf{k}\omega)$ is the hole spectral functions and $n_F(\omega) = [\exp(\omega/T)+1]^{-1}$.

The self-energies in equation (2) read

$$\begin{aligned} \mathrm{Im}\,\Pi(\mathbf{k}\omega) &= \frac{16\pi t^2 J}{N}(\Delta+1+\gamma_{\mathbf{k}})\sum_{\mathbf{k}'}(\gamma_{\mathbf{k}}-\gamma_{\mathbf{k}+\mathbf{k}'})^2 \\ &\quad\times\int_{-\infty}^\infty \mathrm{d}\omega' \left[n_F(\omega+\omega') - n_F(\omega')\right] \\ &\quad\times A(\mathbf{k}+\mathbf{k}', \omega+\omega') A(\mathbf{k}'\omega'), \\ \mathrm{Im}\,\Sigma(\mathbf{k}\omega) &= \frac{16\pi t^2}{N\phi}\sum_{\mathbf{k}'}\int_{-\infty}^\infty \mathrm{d}\omega' \Bigg[\gamma_{\mathbf{k}-\mathbf{k}'} + \gamma_{\mathbf{k}} \\ &\quad + \mathrm{sgn}(\omega')(\gamma_{\mathbf{k}-\mathbf{k}'} - \gamma_{\mathbf{k}})\sqrt{\frac{1+\gamma_{\mathbf{k}'}}{1-\gamma_{\mathbf{k}'}}}\Bigg]^2 \\ &\quad\times[n_B(-\omega') + n_F(\omega-\omega')] \\ &\quad\times A(\mathbf{k}-\mathbf{k}', \omega-\omega') B(\mathbf{k}'\omega'), \end{aligned} \tag{6}$$

where $n_B(\omega) = [\exp(\omega/T)-1]^{-1}$. The source of damping of spin excitations described by equation (6) is the decay into two fermions. Another source of damping, multiple spin excitation scattering, is considered phenomenologically by adding the small artificial broadening $-2\eta\omega_{\mathbf{k}}$, $\eta = 0.02t$ to $\mathrm{Im}\Pi(\mathbf{k}\omega)$. The broadening $-\eta$ is also added to $\mathrm{Im}\Sigma(\mathbf{k}\omega)$ to widen narrow lines and to stabilize the iteration procedure.

The same derivation for the transversal spin Green's function gives $\langle\langle s_{\mathbf{k}}^{-1} | s_{\mathbf{k}}^{+1}\rangle\rangle = 2D(\mathbf{k}t)$ indicating that the used approach retains properly the rotation symmetry of spin components in the paramagnetic state.

For low hole concentrations and temperatures the bandwidth of the dispersion $\varepsilon_{\mathbf{k}}$, equation (3), is approximately equal to t which is much smaller than $8t$, the bandwidth of uncorrelated electrons. The reason for this band narrowing is the antiferromagnetic alignment of spins. In this case the hole movement is accompanied by the spin flipping. In these conditions the hole dispersion is determined by the self-energy $\Sigma(\mathbf{k}\omega)$ which is responsible for a considerable energy gain for states in the spin-polaron band. For the parameters used this gain is approximately equal to $2t$.

3 The hole spectrum

Equations (2–6) form a closed set which was solved by iteration. Examples of the hole spectral functions for the cases of low and moderate doping are given in Figures 1 and 2. The frequency is measured from the chemical potential. For low x the shapes of the spectra are close to those obtained in the spin-wave approximation [8]. As seen from Figure 1, at low doping the hole spectral function contains a series of nearly equidistant maxima. The first member of this series is the narrow peak with the highest intensity which is frequently termed the spin-polaron peak (in some of the spectra in Figures 1 and 2 only its foot is shown). The dispersion of the maxima in the above spectra along the symmetry directions is shown in Figure 3. In the spin-polaron band the lowest energy is reached at $(\pi/2, \pi/2)$. The nearly equidistant location of the maxima is clearly seen in Figure 3a. Besides, we notice that the second maximum in the series has a dispersion which is close in shape to the dispersion of the spin-polaron peak. As follows from Figures 2 and 3b, this maximum is retained at moderate doping in some region of the Brillouin zone.

The nearly equidistant position of the maxima in the low-concentration spectra allows us to connect them with vibronic states of a hole in the region of the perturbed short-range antiferromagnetic order. The moving hole leaves behind it a trace of overturned spins. Such disturbance requires energy which in its turn leads to a restoring force acting on the hole and giving rise to its vibrations. This notion is close to the string picture developed in references [22] for the Ising model and used for the interpretation of the fine spectral structure in the t-J model on small lattices [3,4].

The two lowest maxima of the above-mentioned series are apparently observed in lightly doped $Ca_2CuO_2Cl_2$ [23]. The narrow and intensive spin-polaron peak is responsible for the photoemission maximum with

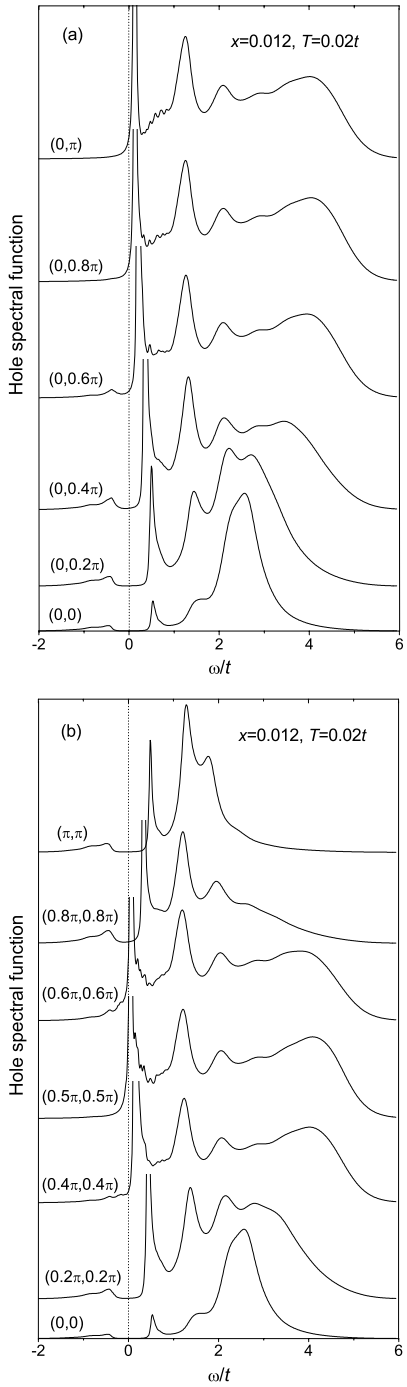

Fig. 1. The hole spectral function $A(\mathbf{k}\omega)$ along the symmetry lines for $x = 0.012$, $T = 0.02t$ and $J/t = 0.2$. The respective values of the wave vectors are indicated near the curves. Here and below the hole picture is used. The vertical dotted line indicates the position of the chemical potential.

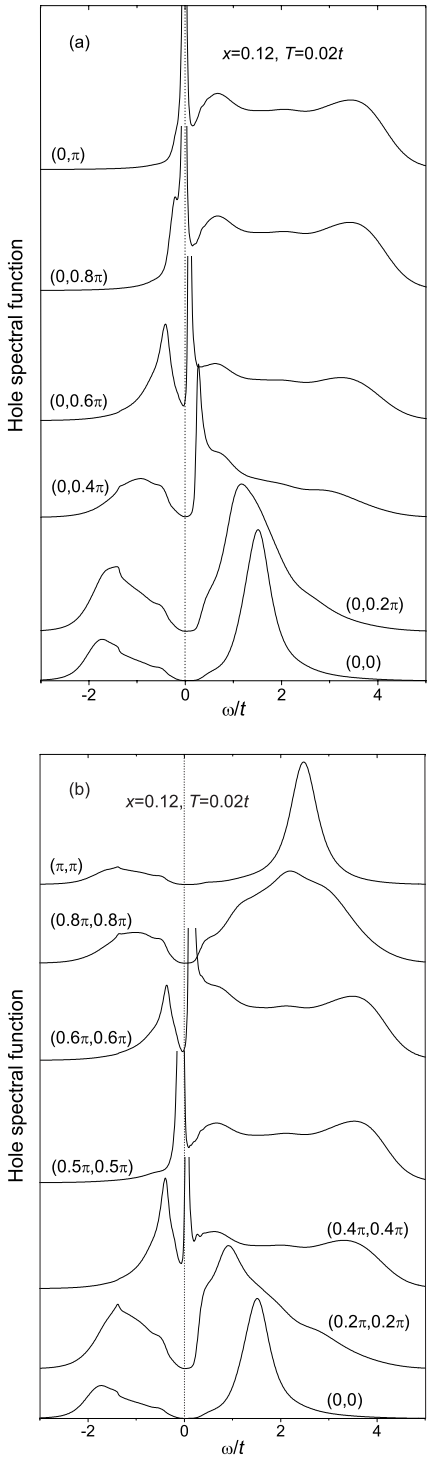

Fig. 2. The hole spectral function for $x = 0.12$ and $T = 0.02t$.

the lowest binding energy, while the second member of the series corresponds to the spectral maximum which is observed at approximately 600 meV higher binding energy. This energy difference is close to that shown in Figure 3a. Besides, as noted in reference [23], the dispersion of the second maximum mimics the dispersion of the spin-polaron peak, which conforms with our calculations. However, it should be noted that our calculated dispersion of the spin-polaron band differs somewhat from that observed experimentally in lightly doped cuprates [23,24]. Although the shapes and magnitudes of the experimental and calculated dispersions along the nodal direction (from $(0,0)$ to (π,π)) are close, along the boundary of the magnetic Brillouin zone (from $(0,\pi)$ to $(\pi,0)$) the magnitude of the calculated dispersion is an order of magnitude

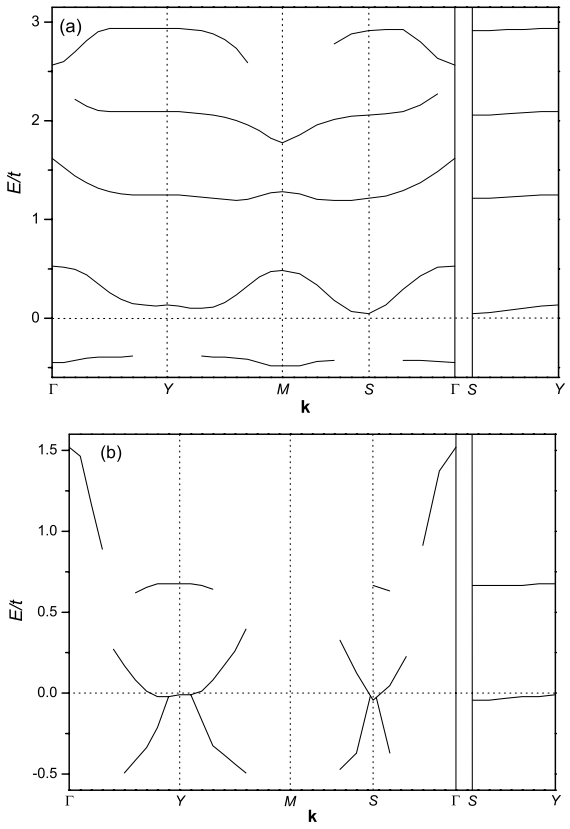

Fig. 3. The dispersion of the maxima in the hole spectral function for $T = 0.02t$, $x = 0.012$ (a) and $x = 0.12$ (b). Points Y, M and S correspond to $\mathbf{k} = (0, \pi)$, (π, π) and $(\pi/2, \pi/2)$, respectively.

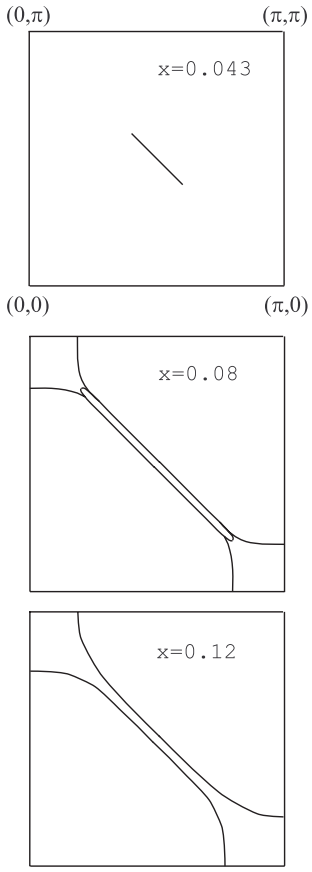

Fig. 4. The Fermi surface in the first quadrant of the Brillouin zone for $x = 0.043$, 0.08, and 0.12. $T = 0.02t$.

smaller than the experimental one. A possible reason for this discrepancy is the oversimplified hole hopping term in Hamiltonian (1) which takes into account the transfer between nearest neighbor sites only [23,25].

The spectral intensity below the chemical potential in Figures 1 and 3a is noteworthy. Already at low x in some region of the Brillouin zone this spectral feature looks like a weak maximum. It is this spectral intensity which provides a finite hole concentration until the spin-polaron band crosses the Fermi level at $x \approx 0.04$.

With increasing x and T the high-frequency maxima in the nearly equidistant series are smeared, as seen in Figure 2. Inspecting this figure one can see that for moderate hole concentrations two maxima – the spin-polaron peak and a less intensive and broader maximum – cross the Fermi level. This latter maximum originates from the mentioned spectral feature which appears below the chemical potential at low x. The dispersions of the two maxima and some other spectral peculiarities are shown in Figure 3b. The maxima can be resolved in the spectrum only in some regions of the Brillouin zone. This is the reason why the curves in Figure 3b terminate at some points of the symmetry lines.

The evolution of the Fermi surface with doping is shown in Figure 4. No Fermi surface exists for $x \lesssim 0.04$, since no maximum which can be identified with a quasiparticle excitation crosses the Fermi level (see Figs. 1 and 3a). As indicated above, for such x the occupied hole states are located at some distance from the level. At $x \approx 0.04$ the spin-polaron band crosses the Fermi level near $(\pm\pi/2, \pm\pi/2)$ which produces a Fermi surface consisting of four strongly elongated ellipses around these points. In Figure 4 the transverse size of one of these ellipses is much smaller than the used momentum step and therefore the ellipse is depicted as a line segment. At $x \approx 0.05$ the second band crosses the Fermi level. With this crossing the Fermi surface acquires new elements – in addition to the ellipses of the spin-polaron band there appear two large rhombuses centered at $(0, 0)$ and (π, π) (see Fig. 4, the case $x = 0.08$). One of these rhombuses can be considered as a shadow image of the other, which arises due to the antiferromagnetic short-range order. Notice, however, that the rhombuses are slightly different in size. In such a manner the small Fermi surface which exists for $x \lesssim 0.05$ is transformed to the large surface for larger hole concentrations. With a further increase of x the Fermi level moves up from the bottom of the spin-polaron band, the size of the ellipses grows and their shape is somewhat changed. At $x \approx 0.12$ they reach the boundaries of the Brillouin zone and the parts of the Fermi surface connected with the spin-polaron band are transformed into two rhombuses the shapes and sizes of which are close to those connected with the second band. Thus,

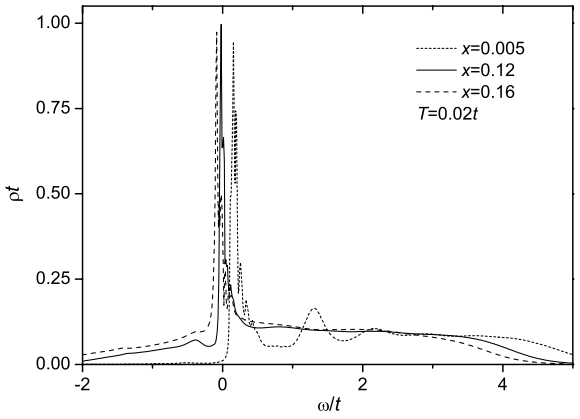

Fig. 5. The normalized hole density of states.

for $x \gtrsim 0.12$ the Fermi surface consists of two rhombuses centered at $(0,0)$ and (π,π) (see Fig. 4).

The compound $Bi_2Sr_2CaCu_2O_{8+\delta}$ is most intensively investigated in angle-resolved photoemission experiments. However, even for this crystal the Fermi surface topology is a topic of an intense controversy (see, *e.g.*, Ref. [26] and references therein). The main reasons for this are broad spectral features in underdoped normal-state crystals and the weak dispersion around $(\pi,0)$ (the so called flat bands or extended van Hove singularities, see Fig. 3b). We notice also that for moderate doping the spin-polaron band in all the area between the rhombuses lies less than 20 meV below the Fermi level. This energy is on the verge of accuracy of photoemission experiments. Nevertheless in the variety of experimental results on the Fermi surface of normal-state cuprates it is possible to find some features which resemble those shown in Figure 4. The shadow Fermi surfaces (together with some other replicas of the main Fermi surface) are observed in $Bi_2Sr_2CaCu_2O_{8+\delta}$ [26,27]. In some experimental conditions in this crystal and in $La_{2-x}Sr_xCuO_4$ the shapes of experimental Fermi surfaces [28,29] are close to that shown in Figure 4 for $x = 0.12$. Notice however that in reference [29] such shape of the Fermi surface in $La_{2-x}Sr_xCuO_4$ is ascribed to dynamic stripes presumed in this crystal.

As indicated, in the range $0.05 \lesssim x \lesssim 0.12$ the Fermi surface contains parts arising due to the crossings of the Fermi level by two different bands. The spectral maxima corresponding to these bands differ essentially in their intensity. In comparison with the spin-polaron peak the spectral maximum of the second band is weaker and broader (see Fig. 2). As a consequence, for wave vectors near $(0,\pi)$ and $(\pi,0)$ this maximum is lost to the foot of the spin-polaron peak on crossing the Fermi level. Since the spin-polaron band lies somewhat above the Fermi level in this region of the Brillouin zone, the situation looks like a part of the Fermi surface disappears here and a gap opens between the hole energy band and the Fermi level [8,30]. In its size (∼20 meV) and symmetry this gap is similar to the pseudogap observed in photoemission spectra. The gap disappears at $x \approx 0.12$ when the whole Fermi surface stems from the crossing of the spin-polaron band with the Fermi level.

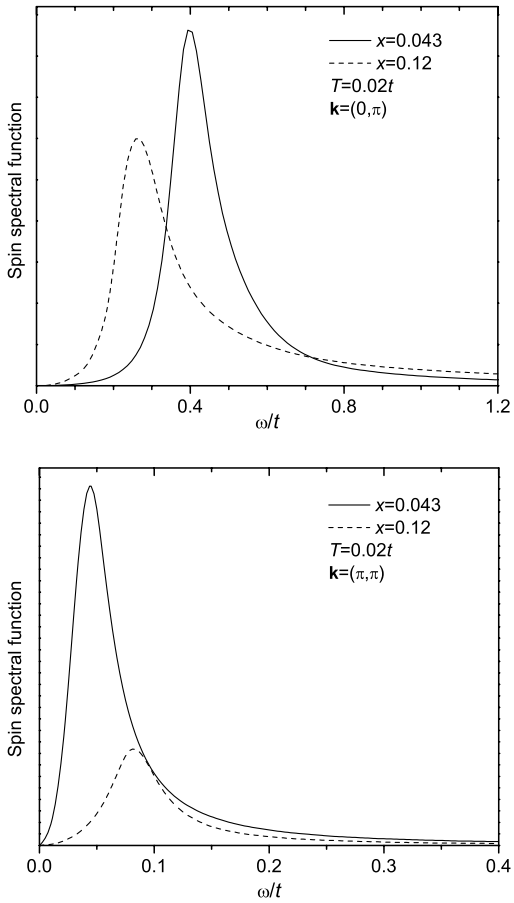

Fig. 6. The spin spectral functions for $\mathbf{k} = (0,\pi)$ and (π,π).

The normalized hole density of states,

$$\rho(\omega) = N^{-1} \sum_{\mathbf{k}} A(\mathbf{k}\omega),$$

is shown in Figure 5 for three hole concentrations from the extremely low to the moderate doping case. As seen from the figure, a considerable part of the density of states is concentrated at a maximum which persists near the Fermi level in a wide range of hole concentrations. This maximum is produced by the above-mentioned extended van Hove singularities in the spin-polaron band and plays a great role in the superconductive transition in the t-J model [31].

4 The spectrum of spin excitations

Typical shapes of the spin spectral function $B(\mathbf{k}\omega)$ are shown in Figure 6. For low and moderate x the spectrum consists of a maximum with an extended high-frequency tail. Some fine structure can be observed for certain wave vectors which is connected with the frequency dependence of the polarization operator (6).

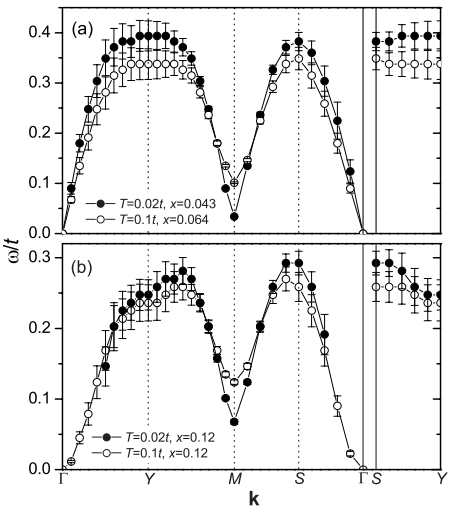

Fig. 7. The dispersion of spin excitations. Vertical bars show decay widths $|\mathrm{Im}\Pi(\mathbf{k}\omega)|/(2\omega_{\mathbf{k}})$. The notations of the symmetry points are the same as in Figure 3.

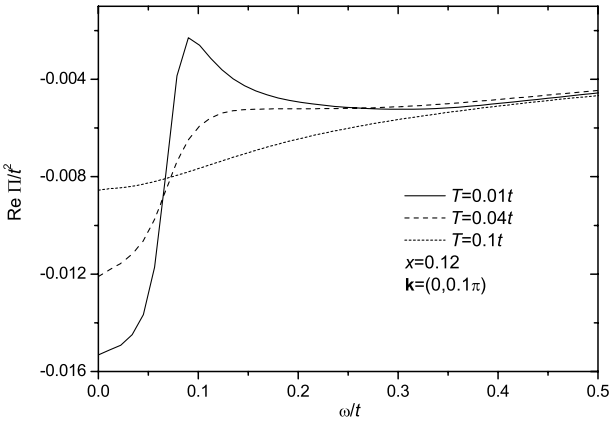

Fig. 8. The real part of the polarization operator $\mathrm{Re}\,\Pi(\mathbf{k}\omega)$ for $\mathbf{k} = (0, 0.1\pi)$, $x = 0.12$ and various temperatures.

The increases of the temperature and the hole concentration act in a similar manner on the spectrum. This action is different in the nearest vicinity of (π, π) and in the remainder of the Brillouin zone. As seen from Figure 6, in the latter case with increasing x (and T) the maximum in $B(\mathbf{k}\omega)$ is shifted to lower frequencies and loses its intensity, while in the former case the frequency of the maximum, on the contrary, grows. This frequency growth is connected with the gap in the spin excitation spectrum at (π, π). The magnitude of this gap grows with increasing x and T.

As follows from equation (2), the frequencies of spin excitations satisfy the equation

$$\omega^2 - \mathrm{Re}\Pi(\mathbf{k}\omega) - \omega_{\mathbf{k}}^2 = 0. \tag{7}$$

Their dispersion along the symmetry lines is shown in Figure 7 for different x and T. In this figure vertical bars depict the decay widths $|\mathrm{Im}\Pi(\mathbf{k}\omega)|/(2\omega_{\mathbf{k}})$ of the excitations, the imaginary parts of the respective poles in Green's function. As seen from Figure 7a, for low x and T the dispersion of spin excitations is close to the dispersion of spin waves. The main difference is the above-mentioned spin gap at (π, π). In an infinite crystal the magnitude of this gap is directly connected with the spin correlation length ξ. Indeed, using equation (2) and taking into account that the region near (π, π) gives the main contribution to the summation over $\mathbf{k}$, we find for large distances and low temperatures

$$\begin{aligned}\langle s_{\mathbf{l}}^z s_{\mathbf{0}}^z\rangle &= N^{-1}\sum_{\mathbf{k}} \mathrm{e}^{\mathrm{i}\mathbf{k}\mathbf{l}} \int_0^\infty \mathrm{d}\omega \coth\left(\frac{\omega}{2T}\right) B(\mathbf{k}\omega) \\ &\propto \mathrm{e}^{i\mathbf{Q}\mathbf{l}}(\xi/|\mathbf{l}|)^{1/2}\mathrm{e}^{-|\mathbf{l}|/\xi}, \\ \xi &= \frac{a}{2\sqrt{\Delta}},\end{aligned} \tag{8}$$

where $\mathbf{Q} = (\pi, \pi)$ and a is the intersite distance (in the considered temperature and hole concentration ranges $\omega_{\mathbf{Q}}^2 \gg |\mathrm{Re}\,\Pi(\mathbf{Q}, \omega_{\mathbf{Q}})|$; therefore in the above equation the gap magnitude is approximated by $\omega_{\mathbf{Q}}$). For low x we found $\Delta \approx 0.2x$ and consequently

$$\xi \approx \frac{a}{\sqrt{x}}.$$

This relation between the spin correlation length and the hole concentration has been experimentally observed in $La_{2-x}Sr_xCuO_4$ [17].

With growing x the spin excitation branch is destroyed in some region around the Γ point – for such momenta equation (7) has no real solution due to a negative value of $\mathrm{Re}\,\Pi(\mathbf{k}\omega)$. In Figure 7 this peculiarity is reflected in the rupture of the dispersion branch in this region where excitation frequencies are purely imaginary. Thus, much like the Heisenberg model [32,33], properties of elementary excitations near $(0, 0)$ and (π, π) are different: in the former region the excitations are overdamped, while in the latter they are gapped. With rise of temperature the branch are partly restored around $(0, 0)$. The explanation for such behavior follows from Figure 8. For low temperatures and long wavelengths $\mathrm{Re}\,\Pi(\mathbf{k}\omega)$ has a pronounced dip at low frequencies. This dip is connected with the spin-polaron band and is responsible for the lack of real solutions in equation (7). With increasing T the spin-polaron peaks are smeared, the depth of the dip in Figure 8 becomes smaller and equation (7) has again real solutions.

5 Magnetic properties

As already mentioned, in accord with the Mermin-Wagner theorem [21] the considered 2D system is in the paramagnetic state for $T > 0$. This result can also be obtained using equations of Section 2. Numerical calculations and the analysis of experimental data presented strong evidence that the 2D nearest-neighbor $s = \frac{1}{2}$ Heisenberg antiferromagnet has long-range order at $T = 0$ [33]. Let us

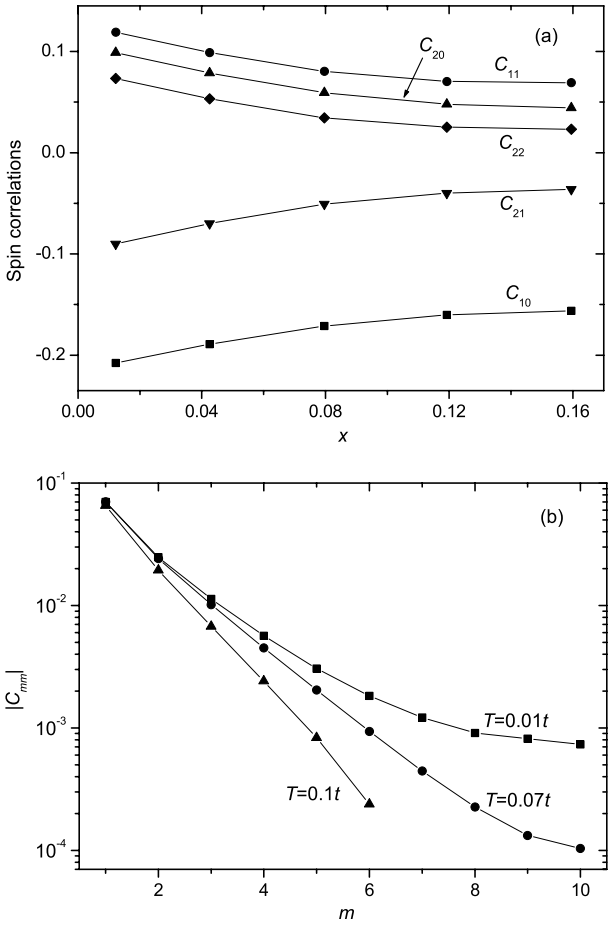

Fig. 9. (a) Spin correlations *vs.* x for $T = 0.02t$. (b) Spin correlations along the diagonal of the crystal (*i.e.* $\mathbf{l} = (m, m)$) for $x = 0.12$. The respective temperatures are indicated near the curves.

consider an infinite crystal at $T = 0$ and find the hole concentration x_c which destroys this ordering. Notice that the indication of the long-range order is a finite value of the condensation parameter C which is determined from constraint (4) and the condition $\Delta = 0$,

$$C = \frac{1}{2}(1-x) - \sqrt{\frac{|C_1|}{\alpha}}\frac{1}{N}\sum_{\mathbf{k}\neq\mathbf{Q}}\sqrt{\frac{1-\gamma_{\mathbf{k}}}{1+\gamma_{\mathbf{k}}}}, \quad N\to\infty. \quad (9)$$

As seen from equations (4) and (9),

$$C = \sqrt{\frac{2|C_1|}{\alpha}}\lim_{N\to\infty}\frac{1}{N\sqrt{\Delta}}.$$

As follows from equation (8), the sublattice magnetization $M = (\lim_{|\mathbf{l}|\to\infty}|\langle \mathbf{s_l}\cdot\mathbf{s_0}\rangle|)^{1/2}$ is connected with the condensation parameter by the relation $M = (3C/2)^{1/2}$. To estimate x_c the dependencies of C_1 and α on x have to be taken into account. From our calculations for low x we found that $|C_1| \approx 0.2117 - 0.5750x$ and $\alpha \approx 1.802 - 8.021x$. Substituting these values into equation (9) we find that C vanishes at $x_c \approx 0.02$. Thus, at $T = 0$ the infinite 2D crystal is in the state with long-range antiferromagnetic order for $x < x_c$ and in the paramagnetic state for $x > x_c$.

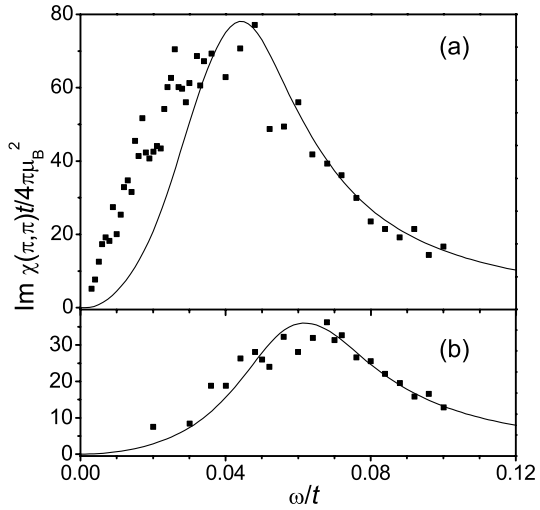

Fig. 10. The imaginary part of the spin susceptibility for $\mathbf{k} = (\pi, \pi)$. Curves show calculated results for $T = 0.02t \approx 116$ K, $x = 0.043$ (a) and 0.08 (b). Squares are experimental results obtained in normal-state $YBa_2Cu_3O_{7-y}$ at $T = 100$ K for $y = 0.5$ (a) and 0.17 (b) [34].

In the considered finite lattice the correlation length is limited by the size of the lattice. The spin correlations $C_{mn} = \langle s^z_{\mathbf{l}} s^z_{\mathbf{0}}\rangle$, $\mathbf{l} = (m, n)$ calculated from the obtained spin spectral function with the use of equation (8) are shown in Figure 9. For large enough x and T the correlations decay exponentially with distance in the considered finite lattice. As mentioned, the method used has no preset magnetic ordering. The character of the ordering is determined in the course of the self-consistent calculations. The magnetic susceptibility obtained in these calculations is strongly peaked at the antiferromagnetic wave vector for low frequencies. No indications of incommensurability, which can be related to stripes or other types of phase separation, are observed in the susceptibility. Conceivably such phase separations are not connected with the strong electron correlations described by the t-J model.

The magnetic susceptibility is connected with the spin Green's function (2) by the relation

$$\chi^z(\mathbf{k}\omega) = -4\mu_B^2 D(\mathbf{k}\omega),$$

where μ_B is the Bohr magneton. Experiments on inelastic neutron scattering give information on the susceptibility which can be directly compared with the calculated results. Such comparison with the results measured in normal-state $YBa_2Cu_3O_{7-y}$ [34] is carried out in Figure 10. $YBa_2Cu_3O_{7-y}$ is a bilayer crystal and the symmetry allows one to divide the susceptibility into odd and even parts. For the antiferromagnetic intrabilayer coupling the odd part can be compared with the calculated results. The oxygen deficiencies $y = 0.5$ and 0.17 in the experimental data in Figure 10 correspond to the hole concentrations $x \approx 0.05$ and 0.11, respectively [35]. As seen from Figure 10, the calculated data reproduce correctly the frequency dependence of the susceptibility, the values of the frequency for which $\mathrm{Im}\chi(\pi, \pi)$

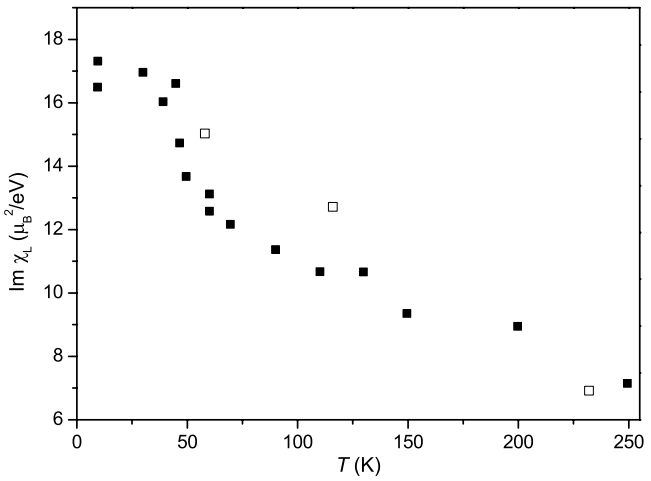

Fig. 11. The local spin susceptibility. The experimental results [34] in $YBa_2Cu_3O_{6.5}$ for $\omega = 25$ meV are shown by filled squares. Our calculated data for $x = 0.05$ and $\omega = 22.5$ meV are displayed by open squares.

reaches maximum and their evolution with doping. The increase of the frequency of the maximum with x reflects the respective growth of the spin gap (see Fig. 6). In absolute units the calculated maxima of $\mathrm{Im}\chi(\pi,\pi)$ are $1.5-2$ times larger than the experimental values which is connected with some difference in decay widths of spin excitations.

The temperature variations of the experimental and calculated susceptibilities are compared in Figure 11. This figure demonstrates the imaginary part of the local spin susceptibility which is defined as

$$\mathrm{Im}\chi_L(\omega) = N^{-1}\sum_{\mathbf{k}} \mathrm{Im}\chi(\mathbf{k}\omega).$$

As seen from the figure, the calculated temperature variation of the susceptibility is also in good agreement with experiment.

The calculated temperature and concentration dependencies of the uniform static spin susceptibility,

$$\chi_0 = \chi(\mathbf{k}\to 0, \omega = 0) = 4\mu_B^2 T^{-1}\sum_{\mathbf{n}} \langle s_{\mathbf{n}}^z s_{\mathbf{0}}^z\rangle\,,$$

are shown in Figure 12. The values lie in the range 2–2.6 eV^{-1} which is close to the values 1.9–2.6 eV^{-1} obtained for $YBa_2Cu_3O_{7-y}$ [36]. Close values of χ_0 were also obtained by the exact diagonalization of small clusters [5]. The temperature dependence of χ_0 has a maximum and the temperature of the maximum T_m grows with decreasing x. Analogous behavior is observed in cuprates for large enough x [37–40]. In Figure 12a $T_m \approx 600$ K which is close to the value observed in $La_{2-x}Sr_xCuO_4$ for comparable hole concentrations [37]. As known, in the undoped antiferromagnet $T_m \approx J$ [41]. On the high-temperature side $\chi_0(T)$ tends to the Curie-Weiss behavior $1/T$.

The decrease of χ_0 below T_m is sometimes considered as the manifestation of the spin gap. In our opinion this

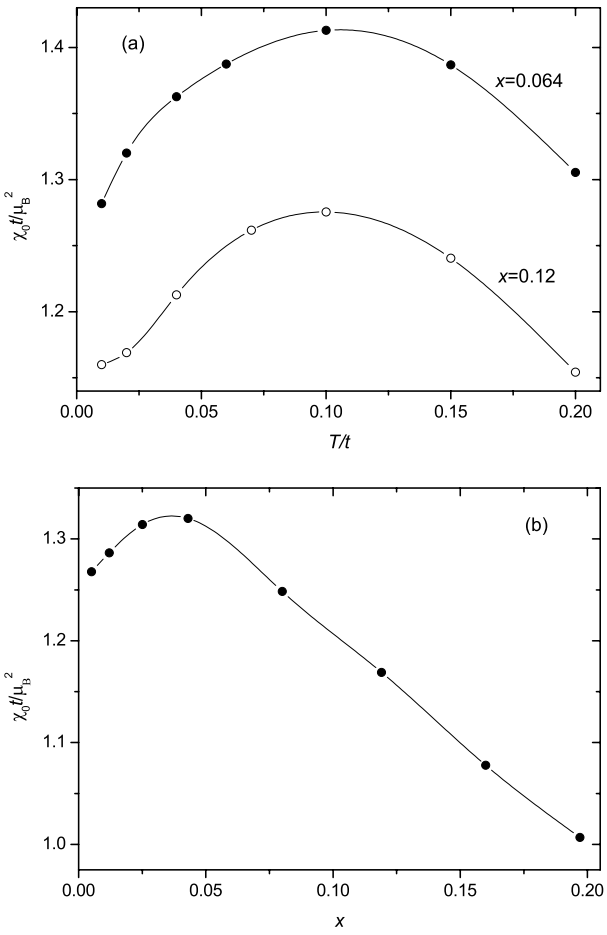

Fig. 12. The uniform static spin susceptibility *vs.* temperature (a) and hole concentration for $T = 0.02t$ (b).

statement is incorrect. For moderate x and T the long-wavelength part of the spin excitation spectrum does not feel the gap at (π,π). For small but finite values of $\mathbf{k}$ $\chi(\mathbf{k},0) \propto \int_{-\infty}^{\infty} \mathrm{d}\omega' B(\mathbf{k}\omega')/\omega'$. As indicated in Section 4, the function $B(\mathbf{k}\omega')$ has a maximum which is shifted to lower frequencies and loses its intensity with increasing temperature for such wave vectors. In the above integral the maximum is superimposed with the decreasing function $1/\omega'$ which finally leads to the nonmonotonic behavior of $\chi_0(T)$.

As seen from Figure 12a, the two curves for the different x are very close in shape and can be superposed by scaling to the same values of the maximum χ_0 and T_m. Analogous scaling was observed in $La_{2-x}Sr_xCuO_4$ [37]. As follows from the above discussion, the source of this scaling is that holes and temperature fluctuations lead in a similar manner to the softening of the maximum in $B(\mathbf{k}\omega')$ for long wavelengths.

As in experiment [37,38], the dependence $\chi_0(x)$ in Figure 12b has a maximum. However, the calculated value of the hole concentration which corresponds to the maximum is much smaller than the experimental value $x \approx 0.25$. A possible reason for this discrepancy is the approximation used for calculating the hole self-energy [11].

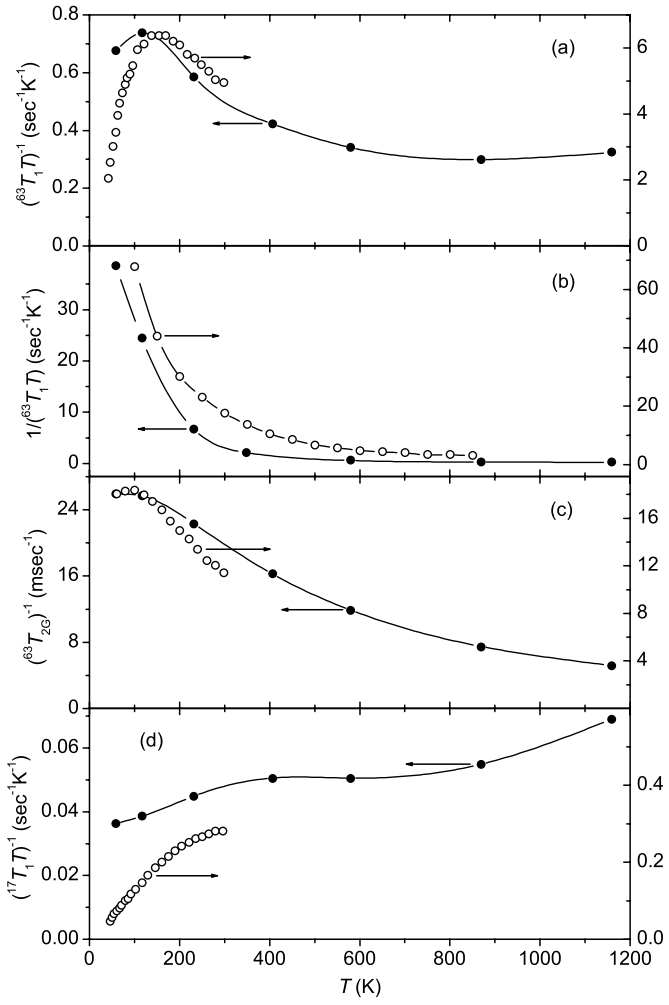

Fig. 13. The temperature dependencies of the spin-lattice relaxation and spin-echo decay rates at Cu (a–c) and O (d) sites. Open circles with right axes represent experimental results, filled circles with left axes are our calculations. (a, c, d) Calculations for $\mathbf{H}\|\mathbf{c}$ and $x = 0.12$, measurements [39,43] in $YBa_2Cu_3O_{6.63}$ ($x \approx 0.1$ [35]). (b) Calculations for nonoriented configuration with $x = 0.043$, measurements [44] in $La_{1.96}Sr_{0.04}CuO_4$.

The spin-lattice relaxation and spin-echo decay rates were calculated with the use of the equations [42]

$$\frac{1}{{}^{\alpha}T_{1\beta}\,T} = \frac{1}{2\mu_B^2 N}\sum_{\mathbf{k}} {}^{\alpha}F_{\beta}(\mathbf{k})\frac{\mathrm{Im}\,\chi(\mathbf{k}\omega)}{\omega}, \quad \omega \to 0,$$

$$\frac{1}{(^{63}T_{2G})^2} = \frac{0.69}{128\mu_B^4}\left\{\frac{1}{N}\sum_{\mathbf{k}} {}^{63}F_e^2(\mathbf{k})\left[\mathrm{Re}\,\chi(\mathbf{k}0)\right]^2 - \left[\frac{1}{N}\sum_{\mathbf{k}} {}^{63}F_e(\mathbf{k})\mathrm{Re}\,\chi(\mathbf{k}0)\right]^2\right\}, \quad (10)$$

where the form factors are

$$\begin{aligned} {}^{63}F_{\|}(\mathbf{k}) &= \left(A_{\perp} + 4B\gamma_{\mathbf{k}}\right)^2, \\ {}^{63}F_e(\mathbf{k}) &= \left(A_{\|} + 4B\gamma_{\mathbf{k}}\right)^2, \\ {}^{63}F_{\perp}(\mathbf{k}) &= \frac{1}{2}\left[{}^{63}F_{\|}(\mathbf{k}) + {}^{63}F_e(\mathbf{k})\right], \\ {}^{17}F_{\|}(\mathbf{k}) &= 2C^2\left(1+\gamma_{\mathbf{k}}\right). \end{aligned} \quad (11)$$

In the above formulas the hyperfine coupling constants $B = 3.82 \times 10^{-7}$ eV, $A_{\perp} = 0.84B$, $A_{\|} = -4B$, and $C = 0.91B$ [42]. The superscripts $\alpha = 63$ or 17 indicate that the respective quantity belongs to the Cu or O site, respectively. The subscripts $\|$ and $\perp$ refer to the direction of the applied static magnetic field $\mathbf{H}$ with respect to the axis $\mathbf{c}$ perpendicular to the Cu-O plane. The form factor ${}^{63}F_e$ is the filter for the Cu spin-echo decay time $^{63}T_{2G}$. Due to the different momentum dependencies of the form factors (11) measurements of the spin-lattice and spin-echo decay rates allow one to extract the information on the low-frequency susceptibility in different regions of the Brillouin zone.

Our calculated results are compared with the respective experimental data in Figure 13. The calculations reproduce satisfactorily the main peculiarities of the temperature dependencies of the spin-lattice relaxation and spin-echo decay rates. The growth of $(^{63}T_1\,T)^{-1}$ with decreasing x is connected with the increase of the spectral intensity of spin excitations near (π,π) which make the main contribution to this rate. For the same hole concentration $(^{63}T_1\,T)^{-1}$ is one order of magnitude larger than $(^{17}T_1\,T)^{-1}$. This is a consequence of the fact that $\mathrm{Im}\,\chi$ is strongly peaked near (π,π) and the momentum dependencies of the form factors (11) [42]. The calculated spin-lattice relaxation rates are smaller than the experimental values due to the approximation made in the calculation of $D(\mathbf{k}\omega)$ which somewhat underestimates $\mathrm{Im}\,\chi$ at low frequencies.

For moderate x with increasing T the low-frequency region of $\mathrm{Im}\,\chi(\mathbf{k}\approx\mathbf{Q})$, $\mathbf{Q} = (\pi,\pi)$ first grows due to the temperature broadening of the maximum in its frequency dependence and then decreases due to the temperature growth of the spin gap (see Fig. 6 and the related discussion). This nonmonotonic behavior of the susceptibility shows up in the spin-lattice relaxation rate at Cu in Figure 13a. The temperature variations of $\mathrm{Im}\,\chi$ and $(^{63}T_1\,T)^{-1}$ can be related with the temperature behavior of the magnetic correlation length. As can be seen in Figure 14, for moderate x and low T the magnitude of the spin gap is determined by the hole concentration and does not depend on T. This temperature range corresponds to the growth stage in Figure 13a. As follows from equation (8), the independence of the gap from T means that in this temperature range ξ does not depend on temperature either which is a distinctive feature of the quantum disordered regime [42,45]. For temperatures above the maximum of $(^{63}T_1\,T)^{-1}$ we found that $^{63}T_1\,T/^{63}T_{2G} \approx$ const. (see Figs. 13a and c). As seen in

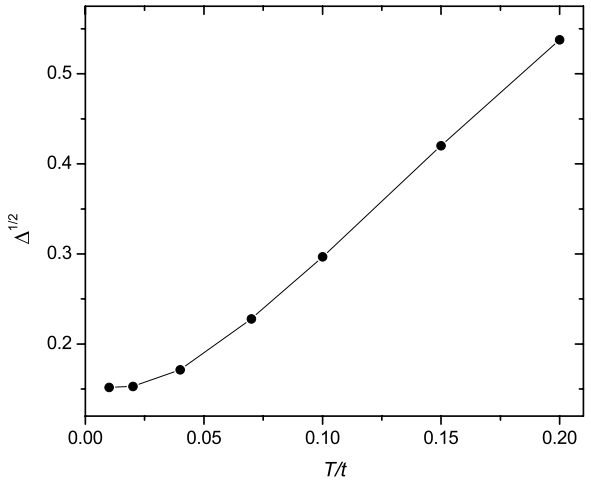

Fig. 14. The temperature dependency of $\sqrt{\Delta} \propto \xi^{-1}$ for $x = 0.12$.

Figure 14, in this temperature range $\xi^{-1} \propto \sqrt{\Delta}$ varies linearly with T. Both these facts indicate that in the mentioned temperature range the crystal is in the quantum critical $z = 1$ regime. These conclusions are consistent with the phenomenological treatment of experiment in $YBa_2Cu_3O_{7-y}$ carried out in reference [42]. The temperature of the maximum in Figure 13a is close to the parameter T_* of that work, the temperature which separates the quantum disordered and quantum critical $z = 1$ regimes.

For small hole concentrations the temperature range in which holes determine the correlation length is absent or very small. In these conditions the spin gap grows starting from low temperatures and $(^{63}T_1\,T)^{-1}$ decreases monotonously, as shown in Figure 13b.

Due to the form factor $^{17}F_{\|}(\mathbf{k})$, equation (11), the momentum region near (π, π) does not contribute to $(^{17}T_1\,T)^{-1}$. As indicated in Section 4, there is a cardinal difference between the behavior of $\mathrm{Im}\,\chi$ for $\mathbf{k} \approx \mathbf{Q}$ and away from (π, π). Due to the spin gap in the former case the frequency of the maximum in $\mathrm{Im}\,\chi(\omega)$ increases with temperature, while in the latter case it decreases. This frequency softening leads to the growth of the low-frequency $\mathrm{Im}\,\chi$ and $(^{17}T_1\,T)^{-1}$ at low T and their saturation for higher temperatures. Analogous behavior is observed in experiment [43], as seen in Figure 13d. Thus, the temperature and concentration variations of the spin excitation spectrum in the t-J model put forward the simple explanations for the behavior of the spin-lattice relaxation and spin-echo decay rates observed in cuprates.

6 Concluding remarks

In this work we applied Mori's projection operator technique and the decoupling of the many-particle Green's functions for obtaining the closed set of self-energy equations which describes energy and magnetic properties of the t-J model of the Cu-O planes in perovskite high-T_c superconductors. The equations retain the rotation symmetry of spin components and zero site magnetization in the paramagnetic state which is set for $T > 0$ or $x > x_c \approx 0.02$ in the case $T = 0$ in an infinite crystal.

For the parameters of cuprates in the cases of low and moderate doping this self-consistently calculated solution of the equations is homogeneous. This result indicates that phase separations are not related to strong electron correlations described by the model.

A number of unusual spectral and magnetic properties of cuprate perovskites is satisfactorily reproduced by the calculations. Among these properties are the extended van Hove singularities around $(0, \pi)$ and $(\pi, 0)$. Due to strong electron correlations these singularities persist near the Fermi level in a wide range of hole concentrations which has to play an essential role in the superconductivity of cuprates.

The pseudogap in the calculated hole spectrum has the same symmetry and is close in magnitude to the pseudogap observed in photoemission of these crystals. As in experiment, the calculated pseudogap disappears when the hole concentration approaches the optimal doping. The existence of two maxima with similar dispersions in the photoemission spectrum of lightly doped $Ca_2CuO_2Cl_2$ is related to hole vibronic states in the region of the disturbed antiferromagnetic order.

In the considered model the concentration dependence of the magnetic correlation length is the same as that observed in $La_{2-x}Sr_xCuO_4$. As indicated, in contrast to this crystal, the model does not show low-frequency incommensurate spin fluctuations for the considered parameters.

In other respects the calculated magnetic susceptibility is close to that derived from experiments. The results of the calculations offer explanations for the observed scaling of the static uniform susceptibility and for the changes in the spin-lattice relaxation and spin-echo decay rates in terms of the temperature and doping variations in the spin excitation spectrum. The scaling is related to the fact that holes and temperature fluctuations lead in a similar manner to the softening of the maxima in the spin spectral function for long wavelengths. This softening leads to the monotonic increase of the spin-lattice relaxation rate at O.

Contrastingly, due to the spin gap the frequencies of the maxima in the spin spectral function for momenta near (π, π) grow with temperature and hole concentration. This region of momenta makes the main contribution to the spin-lattice relaxation rate at Cu. For low hole concentrations the growth of the frequencies of the maxima leads to the monotonic decrease of the rate. For moderate concentrations two temperature regions may be distinguished. In the low-temperature region the gap magnitude and the correlation length depend only weakly on temperature. In this region the spin-lattice relaxation rate at Cu grows. The behavior of these parameters in the high-temperature region is the same as for low hole concentrations.

This work was partially supported by the ESF grant No. 4022 and by DFG.

References

1. P.W. Anderson, Science **235**, 1196 (1987)
2. F.C. Zhang, T.M. Rice, Phys. Rev. B **37**, 3759 (1988)
3. Yu.A. Izyumov, Usp. Fiz. Nauk **167**, 465 (1997) [Phys.-Usp. (Russia) **40**, 445 (1997)]; E. Dagotto, Rev. Mod. Phys. **66**, 763 (1994)
4. E. Dagotto, R. Joynt, A. Moreo, S. Bacci, E. Gagliano, Phys. Rev. B **41**, 9049 (1990)
5. J. Jaklič, P. Prelovšek, Phys. Rev. Lett. **77**, 892 (1996)
6. S.-C. Zhang, J. Carlson, J.E. Gubernatis, Phys. Rev. B **55**, 7464 (1997); M. Calandra, S. Sorella, Phys. Rev. B **61**, R11894 (2000); S. Sorella, G.B. Martins, F. Becca, C. Gazza, L. Capriotti, A. Parola, E. Dagotto, Phys. Rev. Lett. **88**, 117002 (2002)
7. S.R. White, D.J. Scalapino, Phys. Rev. Lett. **80** 1272 (1998)
8. A. Sherman, M. Schreiber, in *Studies of High Temperature Superconductors*, edited by A.V. Narlikar (Nova Science Publishers, New York, 1999), Vol. 27, p. 163; Physica C **303**, 257 (1998); `cond-mat/9808087` (unpublished)
9. N.M. Plakida, Phil. Mag. B **76**, 771 (1997)
10. C.L. Kane, P.A. Lee, T.K. Ng, B. Chakraborty, N. Read, Phys. Rev. B **41**, 2653 (1990); J.P. Rodriguez, B. Doucot, Europhys. Lett. **11**, 451 (1990); X.-G. Wen, P.A. Lee, Phys. Rev. Lett. **76**, 503 (1996)
11. A. Sherman, M. Schreiber, Phys. Rev. B **65**, 134520 (2002)
12. H. Mori, Progr. Theor. Phys. **34**, 399 (1965); A.V. Sherman, J. Phys. A **20**, 569 (1987)
13. J. Kondo, K. Yamaji, Progr. Theor. Phys. **47**, 807 (1972)
14. H. Shimahara, Physica C **185-189**, 1517 (1991); H. Shimahara, S. Takada, J. Phys. Soc. Jpn **61**, 989 (1992); S. Winterfeldt, D. Ihle, Phys. Rev. B **58**, 9402 (1998)
15. A.K. McMahan, J.F. Annett, R.M. Martin, Phys. Rev. B **42**, 6268 (1990)
16. J.M. Tranquada, J.D. Axe, N. Ichikawa, A.R. Moodenbaugh, Y. Nakamura, S. Uchida, Phys. Rev. Lett. **78**, 338 (1997); P. Dai, H.A. Mook, F. Doğan, Phys. Rev. Lett. **80**, 1738 (1998)
17. B. Keimer, N. Belk, R.G. Birgeneau, A. Cassanho, C.Y. Chen, M. Greven, M.A. Kastner, A. Aharony, Y. Endoh, R.W. Erwin, G. Shirane, Phys. Rev. B **46**, 14034 (1992)
18. J.H. Jefferson, H. Eskes, L.F. Feiner, Phys. Rev. B **45**, 7959 (1992)
19. Yu.A. Izyumov, Yu.N. Skryabin, *Statistical Mechanics of Magnetically Ordered Systems* (Consultants Bureau, New York, 1988)
20. H. Shimahara, S. Takada, J. Phys. Soc. Jpn **60**, 2394 (1991)
21. N.D. Mermin, H. Wagner, Phys. Rev. Lett. **17**, 1133 (1966)
22. B. Shraiman, E. Siggia, Phys. Rev. Lett. **60**, 740 (1988)
23. C. Kim, P.J. White, Z.-X. Shen, T. Tohyama, Y. Shibata, S. Maekawa, B.O. Wells, Y.J. Kim, R.J. Birgeneau, M.A. Kastner, Phys. Rev. Lett. **80**, 4245 (1998); F. Ronning, C. Kim, K.M. Shen, N.P. Armitage, A. Damascelli, D.H. Lu, D.L. Feng, Z.-X. Shen, L.L. Miller, Y.-J. Kim, F. Chou, I. Terasaki, `cond-mat/0209651` (unpublished)
24. B.O. Wells, Z.-X. Shen, A. Matsuura, D.M. King, M.A. Kastner, M. Greven, R.J. Birgeneau, Phys. Rev. Lett. **74**, 964 (1995)
25. A.F. Barabanov, V.M. Beresovsky, E. Žąsinas, L.A. Maksimov, Physica C **252**, 308 (1995)
26. A. Damascelli, Z.-X. Shen, Z. Hussain, `cond-mat/0208504` (unpublished)
27. P. Aebi, J. Osterwalder, P. Schwaller, L. Schlapbach, M. Shimoda, T. Mochiku, K. Kadowaki, Phys. Rev. Lett. **72**, 2757 (1994)
28. D.M. King, Z.-X. Shen, D.S. Dessau, D.S. Marshall, C.H. Park, W.E. Spicer, J.L. Peng, Z.Y. Li, R.L. Greene, Phys. Rev. Lett. **73**, 3298 (1994)
29. X.J. Zhou, T. Yoshida, S.A. Kellar, P.V. Bogdanov, E.D. Lu, A. Lanzara, M. Nakamura, T. Noda, T. Kakeshita, H. Eisaki, S. Uchida, A. Fujimori, Z. Hussain, Z.-X. Shen, Phys. Rev. Lett. **86**, 5578 (2001)
30. A. Sherman, M. Schreiber, Phys. Rev. B **55**, R712 (1997)
31. A. Sherman, M. Schreiber, Phys. Rev. B **52**, 10621 (1995); A. Sherman, Phys. Rev. B **55**, 582 (1997)
32. Yu.A. Tserkovnikov, Teor. Mat. Fiz. **52**, 147 (1982) [Theor. Math. Phys. **52**, 712 (1982)]
33. J.D. Reger, A.P. Young, Phys. Rev. B **37**, 5978 (1988); S. Chakravarty, B.I. Halperin, D.R. Nelson, Phys. Rev. B **39**, 2344 (1989)
34. P. Bourges, in *The Gap Symmetry and Fluctuations in High Temperature Superconductors*, edited by J. Bok, G. Deutscher, D. Pavuna, S.A. Wolf (Plenum Press, 1998), p. 349; H.F. Fong, P. Bourges, Y. Sidis, L.P. Regnault, J. Bossy, A. Ivanov, D.L. Milius, I.A. Aksay, B. Keimer, Phys. Rev. B **61**, 14773 (2000)
35. J.L. Tallon, C. Bernhard, H. Shaked, R.L. Hitterman, J.D. Jorgensen, Phys. Rev. B **51**, 12911 (1995)
36. H. Monien, D. Pines, M. Takigawa, Phys. Rev. B **43**, 258 (1991)
37. D.C. Johnston, Phys. Rev. Lett. **62**, 957 (1989)
38. J.B. Torrance, A. Bezinge, A.I. Nazzal, T.C. Huang, S.S.P. Parkin, D.T. Keane, S.J. LaPlaca, P.M. Horn, G.A. Held, Phys. Rev. B **40**, 8872 (1989)
39. M. Takigawa, A.P. Reyes, P.C. Hammel, J.D. Thompson, R.H. Heffner, Z. Fisk, K.C. Ott, Phys. Rev. B **43**, 247 (1991)
40. T. Nakano, M. Oda, C. Manabe, N. Momono, Y. Miura, M. Ido, Phys. Rev. B **49**, 16000 (1994)
41. E. Manousakis, Rev. Mod. Phys. **63**, 1 (1991)
42. V. Barzykin, D. Pines, Phys. Rev. B **52**, 13585 (1995); Y. Zha, V. Barzykin, D. Pines, Phys. Rev. B **54**, 7561 (1996)
43. M. Takigawa, Phys. Rev. B **49**, 4158 (1994)
44. T. Imai, C.P. Slichter, K. Yoshimura, K. Kosuge, Phys. Rev. Lett. **70**, 1002 (1993)
45. A.V. Chubukov, S. Sachdev, J. Ye, Phys. Rev. B **49**, 11919 (1994)